



CrossMark  
 click for updates

Cite this: *RSC Adv.*, 2017, 7, 551

## Ga<sub>2</sub>O<sub>3</sub>–Cu<sub>2</sub>O: synthesis, characterisation and antibacterial properties

Iman A. Hassan,<sup>a</sup> Sanjayan Sathasivam,<sup>ab</sup> Husn-Ubayda Islam,<sup>a</sup> Sean P. Nair<sup>c</sup> and Claire J. Carmalt<sup>\*a</sup>

This paper reports on a Ga<sub>2</sub>O<sub>3</sub>–Cu<sub>2</sub>O composite thin film that allows the destruction of both Gram negative and Gram positive bacteria *via* a dual mechanism involving Ga<sup>3+</sup> ions that disrupt Fe<sup>3+</sup> metabolism pathways in bacteria as well as through the reactive oxygen species generated by possible Fenton type reactions that are mediated by Cu<sup>1+</sup> ions. This dual mechanism allowed the highly transparent composite thin film to destroy both *E. coli* and *S. aureus* to below detection limits in 24 hours and limits the build up of bacterial resistance. The composite film was amorphous and the nature of the Ga and Cu species was extensively analysed on the surface and the bulk using X-ray photoelectron spectroscopy and synchrotron radiation involving linear combination analysis (LCA) and the X-ray absorption near edge structure.

Received 4th October 2016  
 Accepted 10th December 2016

DOI: 10.1039/c6ra24737g

[www.rsc.org/advances](http://www.rsc.org/advances)

### Introduction

Hospital acquired infections (HAI) are a major and increasing problem for hospitals and healthcare institutions globally.<sup>1</sup> The Centers for Disease Control and Prevention (CDC) estimated that 1 in 20 hospitalised patients contracted HAI resulting in approximately 2 million infections contributing to 100 000 deaths a year and costing US hospitals over \$30 billion.

The use of conventional antimicrobials to fight such infections is becoming less effective due to the increasing occurrence of multidrug resistant bacteria.<sup>2,3</sup> Hospital and health care environments represent a reservoir for multidrug resistant bacteria and therefore new methods for reducing or eliminating microorganisms from these environs using antibacterial coatings consisting of (for example) metals and metal oxides with antibacterial properties on high contact touch surfaces, such as keyboards and door handles, is desirable.<sup>4–6</sup>

One of the most well known antibacterial agents is Cu in the metallic or oxide form. It has been used for centuries to decontaminate water. The mode of action is complex, but is believed to be through Fenton type reactions that involve the production of reactive oxygen species (ROS) which go on to cause damage to bacterial cell membranes, DNA and proteins through oxidative stress.<sup>7,8</sup> Although a potent antibacterial agent, Cu and its oxides are expensive relative to other metals

(and metal oxides), thus making the use of Cu costly when application of the coatings on large areas, such as those found in hospitals, is required. Furthermore, the use of Cu or Cu<sub>2</sub>O, CuO causes aesthetic concerns, as the coatings are not transparent but coloured.

Gallium oxide however is highly transparent in the visible and displays antibacterial activity. Ga has demonstrated harmful effects on microorganisms, particularly in mechanisms involving the metabolism of iron.<sup>1</sup> Gallium has been used in biological studies despite having no known physiological functions in the human body. The mechanism for the antimicrobial activity of gallium (Ga<sup>3+</sup>) has been related to its ability to mimic iron (Fe<sup>3+</sup>) but not to participate in redox reactions. Gallium is able to compete with iron and interferes with the absorption and activity of Fe<sup>3+</sup>. Gallium with a trivalent charge (Ga<sup>3+</sup>) has an ionic radius of ~0.55 Å that corresponds well with Fe<sup>3+</sup> (~0.5 Å). This can allow Ga<sup>3+</sup> to displace Fe<sup>3+</sup> in biochemical molecules and pathways. However, iron is redox active but gallium is not. Therefore, the substitution of Fe<sup>3+</sup> with Ga<sup>3+</sup> will lead to the inactivation of Fe-dependent biomolecules. Iron is important for cell division and essential for the formation of DNA. Therefore disruptions in the absorption of iron can cause the cells not to be able to produce sufficient DNA for replication, which ultimately leads to its death.<sup>1–3</sup>

Antimicrobial activity of gallium has been demonstrated with *in vitro* investigation of gallium in the form of gallium maltolate<sup>9,10</sup> and gallium nitrate.<sup>11,12</sup> Studies have shown that gallium nitrate can inhibit the growth of biofilms. Biofilms were grown in the presence and absence of low concentration of gallium nitrate and it was observed that limiting the presence of Fe in the nutrients had a positive correlation with the

<sup>a</sup>Materials Chemistry Centre, Department of Chemistry, University College London, 20 Gordon Street, London WC1H 0AJ, UK. E-mail: [c.j.carmalt@ucl.ac.uk](mailto:c.j.carmalt@ucl.ac.uk); Fax: +44 (0)20 7679 7463

<sup>b</sup>Bio Nano Consulting Ltd, The Gridiron Building, One Pancras Square, London N1C 4AG, UK. E-mail: [info@bio-nano-consulting.com](mailto:info@bio-nano-consulting.com); Fax: +44 (0)20 7396 1056

<sup>c</sup>Division of Microbial Diseases, UCL Eastman Dental Institute, 256 Gray's Inn Road, London, WC1X 8LD, UK



concentration of Ga and microbial reduction was observed. However, when Fe was introduced into the medium, competition between the  $\text{Ga}^{3+}$  and  $\text{Fe}^{3+}$  occurred causing the antimicrobial activity of Ga to decrease.<sup>13,14</sup>

The antimicrobial activity of  $\text{Ga}^{3+}$  was also investigated using  $\text{Ga}_2\text{O}_3$ -doped phosphate-based glasses (PBGs). PBGs are durable materials used as wound dressings where antibacterial ions are incorporated. This unique system would be able to deliver  $\text{Ga}^{3+}$  as the glass degrades. The tests demonstrated that the PBGs had antibacterial effects on different HAI bacterial agents. Results indicated that 1% mol  $\text{Ga}_2\text{O}_3$ -doped PBG was sufficient to be potent against a range of organisms tested. Investigation on  $\text{Ga}_2\text{O}_3$  nanoparticles have shown that they interfere with the adhesion mechanism of bacterial strains and reduce the formation of biofilms.<sup>14</sup>

The use of a composite  $\text{Ga}_2\text{O}_3$ - $\text{Cu}_2\text{O}$  film that contains both Ga and Cu ions would allow a dual mode of attack against bacteria *via* (1) the disruption of bacterial  $\text{Fe}^{3+}$  metabolism by  $\text{Ga}^{3+}$  ions as well as (2) attack through Cu and ROS. Thus making the development of bacterial resistance unlikely. In addition to this, the composite films rich in Ga remain highly transparent in the visible, unlike pure  $\text{Cu}_2\text{O}$  or  $\text{CuO}$  films, therefore allowing application as coatings in hospital and health care environments. In this paper we show the synthesis, to the best of our knowledge, of the first (film or powder) composite  $\text{Ga}_2\text{O}_3$ - $\text{Cu}_2\text{O}$  sample and subsequent tests against both Gram-negative and Gram-positive bacteria. The films were prepared using a novel route called aerosol assisted chemical vapour deposition (AACVD) that is simple and easily scalable.<sup>15–20</sup> Furthermore, since the as-deposited films were X-ray amorphous characterization was carried out using both X-ray photoelectron spectroscopy and linear combination analysis/X-ray absorption near edge structure to determine the nature of Ga and Cu species on the surface and bulk respectively.

## Experimental

### Materials and general methods

The precursor solution for all AACVD depositions was placed in a glass bubbler and vaporised by use of a Vicks ultrasonic humidifier. This produced an aerosol of the precursor in the solvent used. Nitrogen (99.99%) carrier gas was used as supplied from BOC. Depositions were carried out on  $\text{SiO}_2$  coated float-glass that was cleaned using propan-2-ol, acetone and dried in air prior to use. The glass substrates were *ca.* 90 mm  $\times$  45 mm  $\times$  4 mm in size. The heating of the glass substrate to the desired temperature was carried out under nitrogen gas and two-way taps were used to divert the nitrogen carrier gas through the bubbler. The aerosol was carried into the reactor in a stream of nitrogen gas through a brass baffle and a top plate was suspended 0.5 cm above the glass substrate to ensure a laminar flow. After all the precursor solution had passed through the chamber the taps were turned to allow only  $\text{N}_2$  gas flow through the bypass tap. This was maintained until the reaction chamber temperature fell below 100 °C. The  $\text{N}_2$  gas was stopped and the glass substrates were removed. The  $\text{N}_2$  gas flow rate was controlled by a calibrated flow meter positioned

before the gas enters the bypass bubbler. The total deposition time was in the region of 50–80 min.

A graphite block containing a Whatman cartridge heater was used to heat the glass substrate. The temperature of the substrate was monitored by a Pt–Rh thermocouple. Coated substrates were handled and stored in air. Large pieces of glass (*ca.* 4 cm  $\times$  2 cm) were used for X-ray powder diffraction but the coated substrate was cut into *ca.* 1 cm  $\times$  1 cm squares for subsequent analysis.

$\text{GaMe}_3$  were used as supplied from SAFC HiTech.  $\text{GaMe}_3$  is pyrophoric and hence manipulations were performed under a dry, oxygen-free dinitrogen atmosphere using standard Schlenk techniques or in an Mbraun Unilab glovebox. All solvents and alcohols commercially procured from Aldrich were dried with anhydrous engineering equipment and stored in Young's tap flasks.

### Preparation of $\text{Ga}_2\text{O}_3$ film

Dried methanol (30 ml) was added to trimethylgallium [ $\text{GaMe}_3$ , 4.35 mmol] at  $-78$  °C. The resulting solution was mixed under  $\text{N}_2$  for 30 minutes in the AACVD bubbler. The  $\text{Ga}_2\text{O}_3$  films deposited at 450 °C were amorphous.

### Preparation of $\text{Ga}_2\text{O}_3$ - $\text{Cu}_2\text{O}$ film

Copper nitrate trihydrate [ $[\text{Cu}(\text{NO}_3)_2 \cdot 3\text{H}_2\text{O}]$ , 2.06 mmol] was added to dried methanol (30 ml) at room temperature and allowed to dissolve. The copper nitrate solution was then slowly added to  $\text{GaMe}_3$  (4.35 mmol) at  $-78$  °C. After 30 minutes of mixing the solution was used for an AACVD experiment. An aerosol was generated at room temperature. A graphite heating block under the glass substrate heated the CVD reactor to 450 °C. Once deposition was complete, the substrate was cooled to room temperature under  $\text{N}_2$ . The film deposition time was one hour and transparent films covering the glass substrate were produced.

Both films were also deposited on quartz substrates and annealed at 1000 °C for 12 hours under air to subsequently determine the crystallographic phase through X-ray diffraction.

### Characterisation of thin films

The resulting thin films were handled and stored in air. The coated glass substrates were used for powder X-ray diffraction (XRD) measured on a Bruker D8 X-ray diffractometer with  $\text{CuK}\alpha_1$  and  $\text{CuK}\alpha_2$  radiation of wavelength 0.154056 and 0.154439 nm respectively emitted with an intensity ratio of 2 : 1, a voltage of 40 kV and current of 40 mA. The samples were indexed using the GSAS programme, refined *via* the Rietveld method (LeBail model), and compared to database standards. Energy dispersive X-ray analysis (EDX) was obtained on Philips XL30ESEM instrument and Scanning electron microscopy (SEM) on a JEOL 6301 instrument. X-ray photoelectron spectroscopy (XPS) was performed using a Thermo Scientific K-alpha photoelectron spectrometer using monochromatic  $\text{Al}_{K\alpha}$  radiation. Samples were earthed using copper tape. Higher resolution scans were recorded for the principal peaks of  $\text{Cu}(2p)$ ,  $\text{Ga}(3d, 2p)$ ,  $\text{O}(1s)$  and  $\text{C}(1s)$  at a pass energy of 50 eV. The peaks



were modelled using CasaXPS software with binding energies adjusted to adventitious carbon (284.5 eV) for charge correction.

X-ray absorption spectroscopy (XAS) measurements on the Dutch-Belgian Extended X-ray absorption fine structure (EXAFS) beamline (BM26A) at the ESRF in Grenoble. Monochromatic radiation was supplied by a double Si(111) crystal, and fluorescence was measured using a 9 element germanium solid state detector. XAS of the film was acquired in fluorescence. Measurements of the thin film and pelletized copper standards were taken on the copper K-edge (8987 eV). XAS data were processed and X-ray absorption near edge structure (XANES) analysis was performed using Horae Athena software, and detailed EXAFS analysis was performed on Excurve version 9.273.

### Antimicrobial testing

*E. coli* strain (ATCC 25922) and *S. aureus* (8325-4) was maintained by weekly subculture on Brain Heart Infusion (BHI) agar (Oxoid, Basingstoke, UK). One bacterial colony of either *E. coli* or *S. aureus* was used to inoculate 10 ml of sterile BHI broth (Oxoid, Basingstoke, UK) and incubated aerobically at 37 °C for 24 hours. Bacteria from the overnight culture were harvested by centrifugation at  $13\,000 \times g$  for 1 minute. Bacteria were then re-suspended in phosphate-buffered saline (PBS) (Oxoid, Basingstoke, UK) and again centrifuged for  $13\,000 \times g$  for 1 minute. Finally the bacterial pellet was re-suspended in PBS before use. The turbidity of the bacterial cell suspension was measured at 600 nm using a spectrophotometer and was adjusted to an optical density which corresponded to approximately  $10^5$  colony forming units (cfu) per 25  $\mu$ L aliquot.

Prior to use, the gallium oxide and copper gallium oxide samples were cut into  $1 \times 1$  cm sections. A humidity chamber was created to ensure that the suspensions did not dry out. For each exposure time, triplicate samples were analysed and uncoated barrier glass pieces were used as a control. Each exposure time was also repeated twice. A 25  $\mu$ L aliquot of the bacterial cell suspension was spread evenly on the surface of each slide and incubated at room temperature ( $21 \pm 2$  °C) for the allocated exposure time. After incubation the slides were aseptically transferred to 225  $\mu$ L PBS and vortexed for 30 seconds to release the bacteria into the solution. Serial dilutions of the resulting bacterial suspensions were prepared in PBS and 25  $\mu$ L from each dilution was spread on to MacConkey Agar (Oxoid, Basingstoke, UK) for *E. coli* and BHI agar (Oxoid, Basingstoke, UK) for *S. aureus*. Plates were allowed to dry before inverting and incubating aerobically at 37 °C for 24 hours. After incubation, any bacterial colonies were counted and the viable count calculated. The Mann–Whitney *U* test was used to determine the significance of the antimicrobial activity of gallium oxide and copper gallium oxide compared to the control glass slide. As well as, determining the significance of the activity of gallium oxide compared to the copper–gallium oxide.

## Results and discussion

Pure  $\text{Ga}_2\text{O}_3$  and composite  $\text{Ga}_2\text{O}_3\text{-Cu}_2\text{O}$  thin films were deposited on glass substrates *via* aerosol assisted chemical

vapour deposition of  $\text{GaMe}_3$  (4.35 mmol) and  $[\text{Cu}(\text{NO}_3)_2 \cdot 3\text{H}_2\text{O}]$  (2.06 mmol) in dry methanol. Deposition temperature of 450 °C was chosen as it allowed both precursors to decompose efficiently, promoting surface reactions while minimizing gas phase decomposition resulting in complete coverage of the substrate. The films were highly transparent in the visible. Both films passed the Scotch™ tape test and were resistant to marking and delamination when scratched with stainless steel and brass styluses. The films also remained unchanged after suspension in water and organic solvents (methanol and acetone) for 16 hours. In fact they were only damaged by concentrated (nitric) acid (less than two hours). The highly robust nature of the films is an important property that makes them suitable as functional coatings on high contact touch surfaces.

The deposited films were amorphous when probed using X-ray diffraction spectroscopy. This is expected as  $\text{Ga}_2\text{O}_3$  and related systems only exhibit crystallinity at temperatures of 700 °C and above. Annealing of the as-deposited thin films at 1000 °C (to maximize crystallinity) in air for 12 hours did indeed produce crystalline  $\beta\text{-Ga}_2\text{O}_3$ .

The composite film, when annealed, showed the growth of the  $\beta\text{-Ga}_2\text{O}_3$  and CuO phases (Fig. 1). There was no evidence for the formation of the spinel phase that has previously been isolated for AACVD synthesized  $\text{Ga}_2\text{O}_3$  and CuO composite films when annealed under vacuum.<sup>21</sup> As a result, further discussion in this manuscript will focus solely on the amorphous as-deposited films of pure  $\text{Ga}_2\text{O}_3$  and composite  $\text{Ga}_2\text{O}_3\text{-Cu}_2\text{O}$ .

Energy dispersive X-ray spectroscopy (EDX) showed the composite film to be rich in Ga with only 21 at% being composed of Cu compared to 79 at% Ga. The composite film being Cu poor allows it to remain highly transparent without any colour thus enabling it to be applied as a coating on a wider range of surfaces without any issues with aesthetics.

The nature of the Ga and Cu species on the surface of the amorphous composite film was determined by X-ray

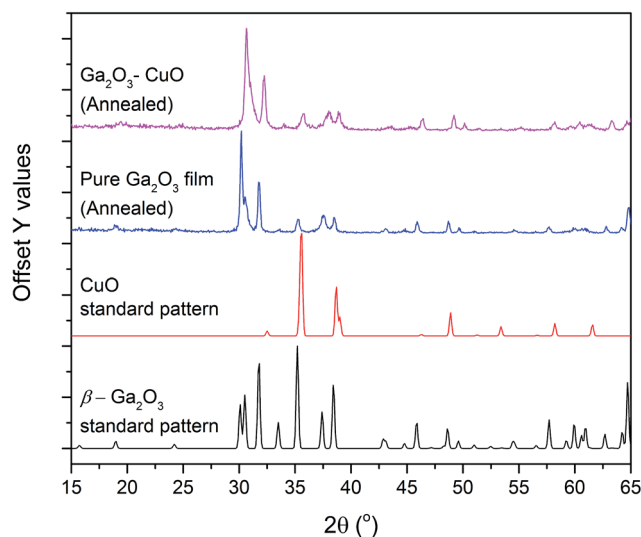


Fig. 1 PXRD patterns of the annealed pure and composite film. The standard patterns for  $\beta\text{-Ga}_2\text{O}_3$  and CuO are also shown.



photoelectron spectra (XPS). The Ga  $2p_{3/2}$  and  $3d_{5/2}$  transitions appear at 1117.9 and 19.9 eV, matching well with literature reports for Ga<sup>3+</sup>.<sup>22,23</sup> The Cu  $2p$  spectrum shows two symmetrical peaks separated by 19.6 eV with a low signal to noise ratio. The Cu  $2p_{3/2}$  peak centered at 932.6 eV can correspond to Cu<sup>0</sup> and/or Cu<sup>1+</sup> as both peaks overlap heavily.<sup>24,25</sup> The ratio of Ga to Cu on the surface was 7 (86 at%) to 1 (14 at%). This is slightly different to what was observed from EDX, which suggests that there was more Cu present in the bulk of the films compared to the surface. The valence band XPS spectra for both films is shown in Fig. 2d. The valence band of pure Ga<sub>2</sub>O<sub>3</sub> is broad, with a width of *ca.* 10 eV and generalized gradient approximation GGA of density functional theory (DFT) suggests that it is primarily composed of O  $2p$  states.<sup>26</sup> Other calculations (tight binding) have however suggested that the valence band of Ga<sub>2</sub>O<sub>3</sub> may also consist of O  $2p$ , Ga  $4p$  and Ga  $4s$  states.<sup>26,27</sup> The composite film shows a similar spectrum to the pure film but is shifted to lower binding energies by *ca.* 1 eV.

The oxidation of the Cu and Ga species in the bulk of the pure Ga<sub>2</sub>O<sub>3</sub> and composite Ga<sub>2</sub>O<sub>3</sub>-Cu<sub>2</sub>O films were analysed using linear combination analysis (LCA) and X-ray absorption near edge structure (XANES). Cu K-edge XANES data for the sample is shown in Fig. 3 along with the corresponding data for

standard powders: Cu, Cu<sub>2</sub>O and CuO. The energy scales of all the spectra have been consistently normalised. Fig. 3 shows that the local environment of Cu can have an effect on the line shape of the XANES spectra, therefore making it fairly simple to identify the nature of Cu present in the Ga<sub>2</sub>O<sub>3</sub>-Cu<sub>2</sub>O films. The prominent feature seen in the Cu K-edge spectra (Fig. 3a) is from the allowed  $1s$  to  $4p$  transition.<sup>28</sup> A low energy peak situated at *ca.* 8982 eV matches for Cu(0) species in the Cu standard powder, this peak is shifted to a higher energy of *ca.* 8985 eV and *ca.* 8987 eV for Cu(I) (Cu<sub>2</sub>O standard powder) and Cu(II) (CuO standard powder) respectively. All these peak positions match closely with literature reports.<sup>28,29</sup>

In this case, the XANES spectra for the amorphous Ga<sub>2</sub>O<sub>3</sub>-Cu<sub>2</sub>O films match that of Cu, Cu<sub>2</sub>O and CuO standards indicating that copper is present in the film in all three oxidation states. This is in contrast to the surface of the film that XPS analysis showed to be lacking in CuO. LCA for the Ga<sub>2</sub>O<sub>3</sub>-Cu<sub>2</sub>O (Table 1) calculated the Cu : Cu<sub>2</sub>O : CuO ratio present in the film is 0.37 : 0.60 : 0.03. The XANES data indicates that Cu, Cu<sub>2</sub>O and a very small amount CuO were identified. XPS only identified the presence of Cu<sub>2</sub>O on the surface of the material. This could be due to CuO not being present at the surface but can be detected in the bulk of the film. The LCA also shows that

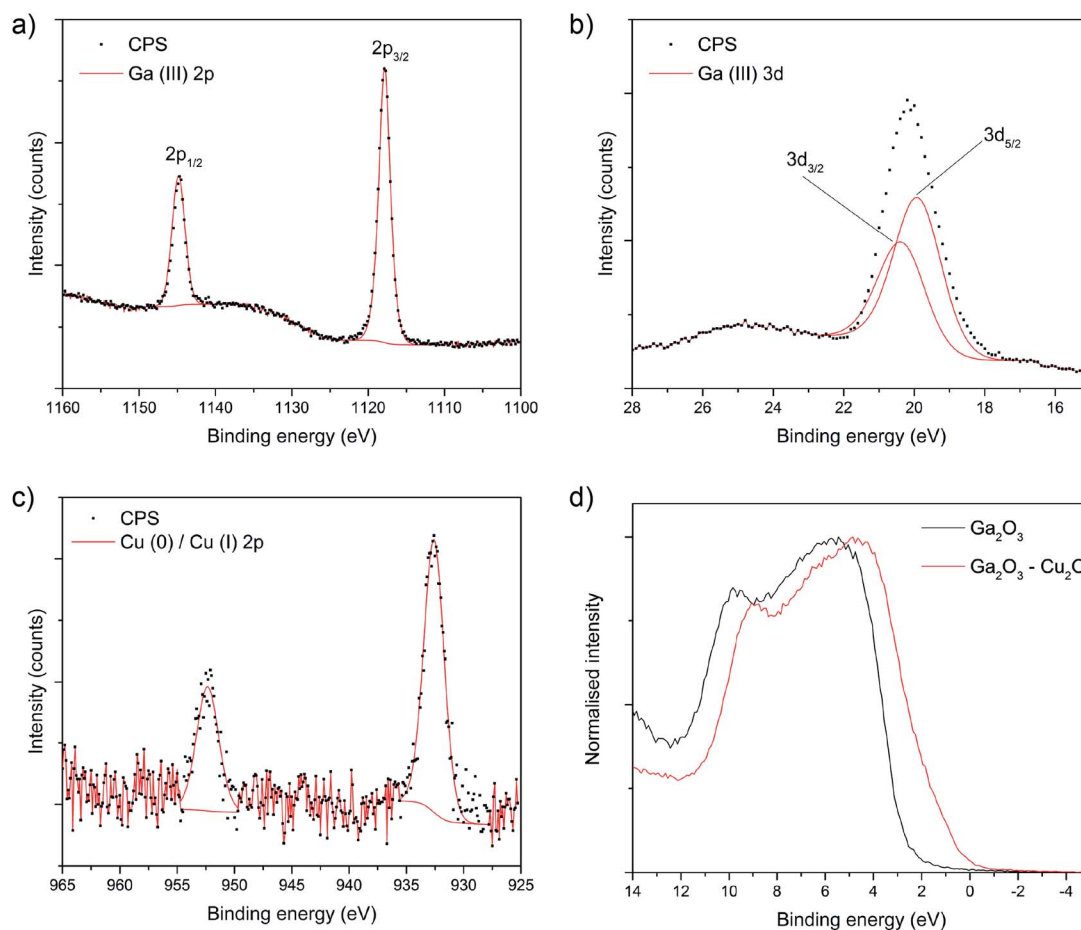


Fig. 2 XPS core level spectra for the composite film showing the (a) Ga  $2p$ , (b) Ga  $3d$  and (c) Cu  $2p$  transitions. (d) Shows the valence band spectra.



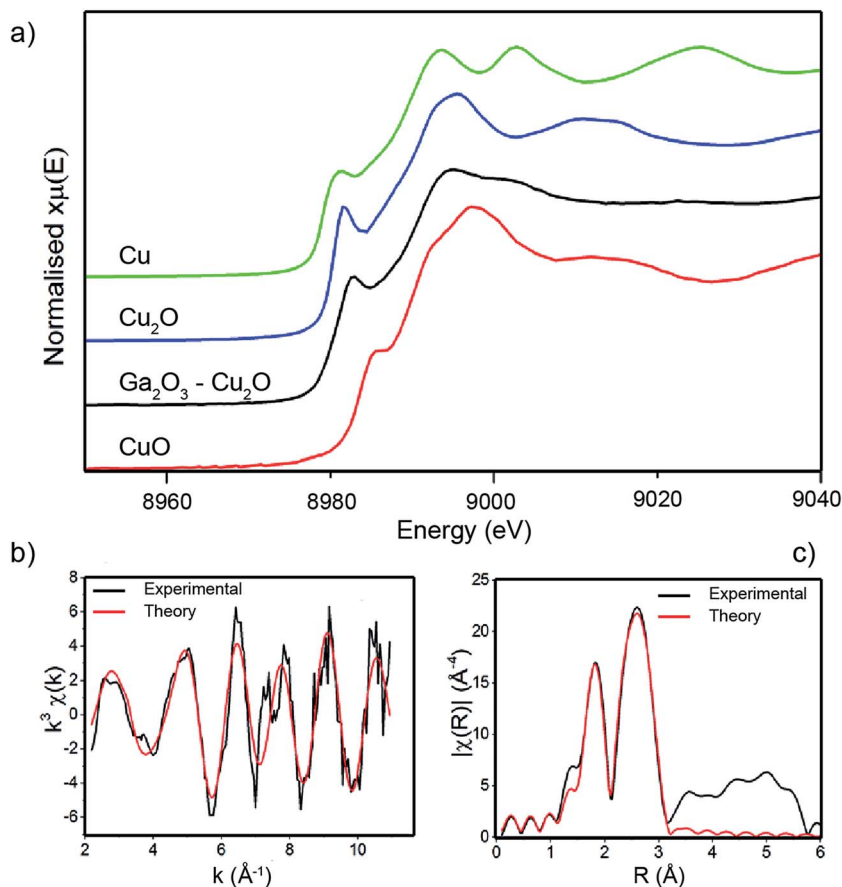


Fig. 3 (a) Normalised Cu K-edge XANES spectra for Cu metal foil,  $\text{Cu}_2\text{O}$ , CuO and the  $\text{Ga}_2\text{O}_3\text{-Cu}_2\text{O}$  composite thin film. (b)  $k^3$ -weighted  $\chi(k)$  spectra  $\text{Ga}_2\text{O}_3\text{-Cu}_2\text{O}$  and theoretical fit. (c) Fourier transform of EXAFS of the  $\chi(k)$ .

Table 1 Linear combination analysis (LCA) of XANES fit for the amorphous  $\text{Ga}_2\text{O}_3\text{-Cu}_2\text{O}$  composite film grown via AACVD at 450 °C

#### LCA of XANES of $\text{Ga}_2\text{O}_3\text{-Cu}_2\text{O}$

Standard	Ratio	R-factor
$\text{Cu}_2\text{O}$	0.60 (0.03)	$2.51 \times 10^{-4}$
CuO	0.03 (0.02)	
Cu	0.37 (0.02)	

#### EXAFS fit of $\text{Ga}_2\text{O}_3\text{-Cu}_2\text{O}$

Scatter	$N$	$R_{\text{XRD}}$ ( $\text{\AA}$ )	$R_{\text{EXAFS}}$ ( $\text{\AA}$ )	$\sigma^2$ ( $\text{\AA}^2$ )	$F$
O	2.0	1.85 ( $\text{Cu}_2\text{O}$ )	1.87 (0.03)	0.010	12
		1.95 (CuO)			
Cu	4.6	2.54 (Cu)	2.55 (0.02)	0.010	

$\text{Cu}_2\text{O}$  has the largest amount in the ratio, which corresponds to the identification that the composite is a  $\text{Ga}_2\text{O}_3\text{-Cu}_2\text{O}$  material.

EXAFS were analysed and revealed the presence of two distances (Table 1). The local structure of  $\text{Cu}_2\text{O}$  with two Cu–O distances that were found to be 1.87  $\text{\AA}$ , which corresponds to bond distances found in  $\text{Cu}_2\text{O}$  (1.85  $\text{\AA}$ ). The Cu–Cu distances

were identified as 2.55  $\text{\AA}$ , which is comparable to Cu–Cu bond distance found in pure copper films (2.54  $\text{\AA}$ ).

An important factor that determines efficiency of antibacterial coatings is the surface area. A more nano- and micro-structured morphology of an active film allows it to rapidly destroy bacteria purely through increased contact. This is the primary reason why nano powders show increased activity compared to bulk powders of the same materials. Scanning electron microscopy (SEM) was used to determine the surface topography of both the as-deposited  $\text{Ga}_2\text{O}_3$  and  $\text{Ga}_2\text{O}_3\text{-Cu}_2\text{O}$  amorphous films and give only a qualitative indication of the differing surface area. The  $\text{Ga}_2\text{O}_3$  film consists of fused particles roughly 100 nm in diameter. This film appeared to have a larger surface area compared to the composite film that showed much larger particle sizes at 400 nm (Fig. 4). Cross sectional SEM imaging showed both films to be 500 nm thick.

Optical properties of the  $\text{Ga}_2\text{O}_3$  and composite  $\text{Ga}_2\text{O}_3\text{-Cu}_2\text{O}$  were studied by transmission and reflectance measurements between 300–2500 nm by UV-Vis spectroscopy (Fig. 5). Both of the amorphous films showed a slight shift in the adsorption edge towards the visible relative to plain glass substrate and displayed minimal reflectively (10–20%). The  $\text{Ga}_2\text{O}_3$  films displayed high transmission (85–90%) whereas the composite was slightly lower in transmission (80–85%).



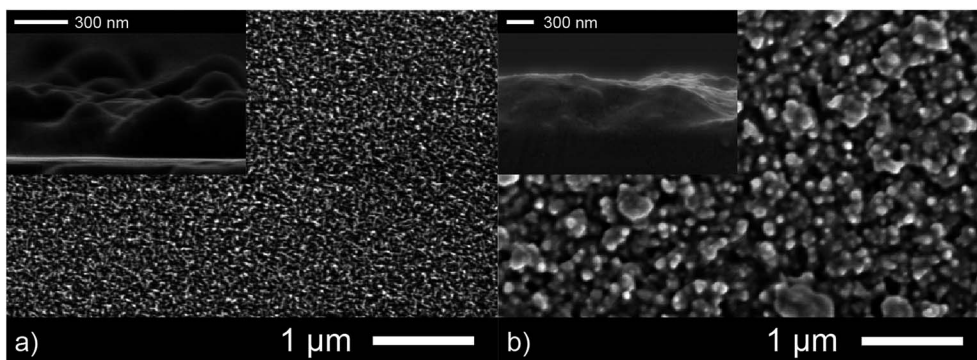


Fig. 4 SEM images of the (a) pure  $\text{Ga}_2\text{O}_3$  film and (b) composite  $\text{Ga}_2\text{O}_3\text{-Cu}_2\text{O}$  grown via AACVD on glass substrates from the reaction of  $\text{GaMe}_3$  and  $\text{Cu}(\text{NO}_3)_2 \cdot 3\text{H}_2\text{O}$  in methanol. The cross-sectional SEM image of each film is also shown as an inset.

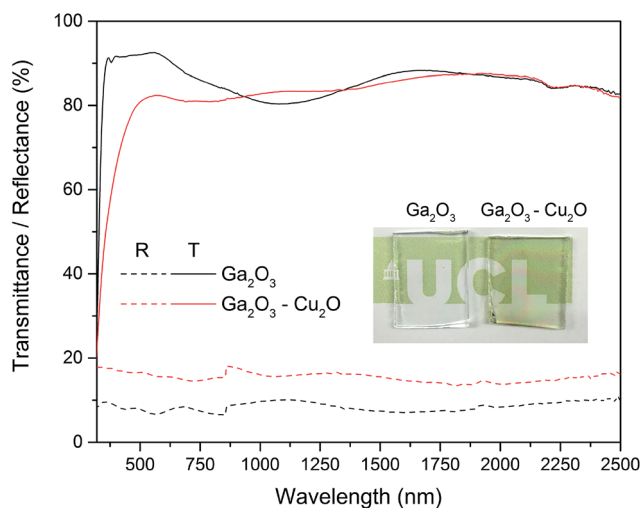


Fig. 5 UV-Vis spectra for the pure  $\text{Ga}_2\text{O}_3$  and the composite  $\text{Ga}_2\text{O}_3\text{-Cu}_2\text{O}$  thin films grown on glass from the AACVD reaction of  $\text{GaMe}_3$  and  $\text{Cu}(\text{NO}_3)_2 \cdot 3\text{H}_2\text{O}$  in methanol at  $450^\circ\text{C}$ . Inset is a photograph of the films showing the high transparency in the visible.

The antimicrobial properties of the amorphous  $\text{Ga}_2\text{O}_3$  and  $\text{Ga}_2\text{O}_3\text{-Cu}_2\text{O}$  films deposited from  $\text{GaMe}_3$  in methanol or a mixture of  $\text{GaMe}_3$  and  $[\text{Cu}(\text{NO}_3)_2 \cdot 3\text{H}_2\text{O}]$  via AACVD at  $450^\circ\text{C}$  were tested against *E. coli* and *S. aureus*. Samples were cut in  $1 \times 1$  cm sample sections and were covered with  $25 \mu\text{L}$  of bacterial cell suspension containing approximately  $10^5$  cfu. Through enumeration and plating of the bacterial suspensions and subsequent overnight incubation ( $37^\circ\text{C}$ ), the resultant viable counts of bacteria for each sample section was determined. The results for the  $\text{Ga}_2\text{O}_3$  and  $\text{Ga}_2\text{O}_3\text{-Cu}_2\text{O}$  films, shown in Fig. 5, demonstrate that the films have antimicrobial activity against *E. coli* and *S. aureus*. Glass cut into  $1 \times 1$  cm were used as controls. Each point represents the  $\log_{10}$  of the mean number of viable bacteria from three samples and error bars represent the standard error. The results for the films show that having both Ga and Cu in the films has an enhancing effect on the antimicrobial activity.

For *E. coli*, a  $0.9 \log_{10}$  reduction ( $P < 0.01$ ) in viable bacteria was observed after 24 hours, for  $\text{Ga}_2\text{O}_3$ , as shown in Fig. 6a. In

the case of  $\text{Ga}_2\text{O}_3\text{-Cu}_2\text{O}$ , the same reduction in colony counts was achieved after only 9 hours ( $P < 0.001$ ) and  $4 \log_{10}$  reduction was observed after 24 hours. This was similar for *S. aureus*, a  $1.2 \log_{10}$  reduction ( $P < 0.001$ ) for  $\text{Ga}_2\text{O}_3$  was observed after 24 hours however, for the  $\text{Ga}_2\text{O}_3\text{-Cu}_2\text{O}$  samples a  $0.8 \log_{10}$  reduction was observed after 9 hours ( $P < 0.001$ )

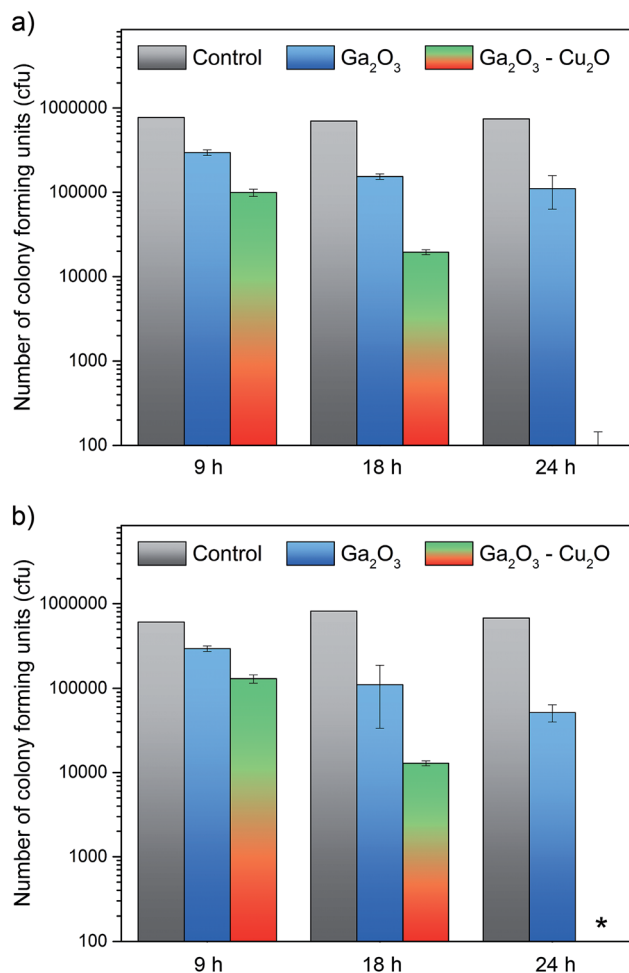


Fig. 6 The antibacterial properties of the pure  $\text{Ga}_2\text{O}_3$  and composite  $\text{Ga}_2\text{O}_3\text{-Cu}_2\text{O}$  thin films as tested against (a) *E. coli* and (b) *S. aureus*.



and 4 log<sub>10</sub> reduction after 24 hours ( $P < 0.001$ ). When the antimicrobial activity of the Ga<sub>2</sub>O<sub>3</sub> thin films prepared in this study are compared to previous studies where Ga<sub>2</sub>O<sub>3</sub>-doped phosphate-based glasses were tested against *Pseudomonas aeruginosa* a similar reduction in the viable count was seen (0.86 log<sub>10</sub> reduction).<sup>9,10</sup> Overall Ga<sub>2</sub>O<sub>3</sub> has been demonstrated to have some antimicrobial activity. With the Ga<sub>2</sub>O<sub>3</sub>-Cu<sub>2</sub>O film, a much greater bacterial reduction was observed. When comparing the difference in the viable count between Ga<sub>2</sub>O<sub>3</sub> and Ga<sub>2</sub>O<sub>3</sub>-Cu<sub>2</sub>O, it was seen to be highly statistically significant ( $P < 0.001$ ) demonstrating the impact of copper on the sample. The Ga<sub>2</sub>O<sub>3</sub>-Cu<sub>2</sub>O has a much improved antimicrobial efficacy over Ga<sub>2</sub>O<sub>3</sub> due to the addition of an antimicrobial metal, copper in a mixture of Cu<sub>2</sub>O. Copper has been shown to produce highly significant reductions in the number of bacteria responsible for HAI. The results herein show that Ga<sub>2</sub>O<sub>3</sub>-Cu<sub>2</sub>O coatings have lower antimicrobial activity compared to Cu and Cu<sub>2</sub>O coatings.<sup>5</sup> It has been shown that copper coatings can reduce bacterial numbers in 30 minutes rather than 24 hours. However, the Ga<sub>2</sub>O<sub>3</sub>-Cu<sub>2</sub>O films we developed were transparent and have the potential to be deposited on a wide variety of surfaces.

## Conclusions

In conclusion we report the first synthesis and material characterization of a Ga<sub>2</sub>O<sub>3</sub>-Cu<sub>2</sub>O composite. The amorphous thin films were characterized using XPS to indicate that the surface was composed of Ga and Cu in the 3+ and 1+ oxidation state at a ratio of 7 : 1. The bulk of the film was determined *via* LCA and XANES analysis to consist of Ga<sup>3+</sup> and primarily Cu<sup>1+</sup>. A small amount of Cu<sup>0</sup> and Cu<sup>2+</sup> was also found. The presence of both Ga<sup>3+</sup> and Cu<sup>1+</sup> in the composite film allowed it to display superior antibacterial activity against both Gram negative (*E. coli*) and Gram positive (*S. aureus*) bacteria with kills to below the detection limits obtained within 24 hours. Whereas the pure Ga<sub>2</sub>O<sub>3</sub> film tested under the same conditions showed only a ~1 log<sub>10</sub> reduction over this time period. The enhanced activity of the composite film was attributed to the dual mechanism of attack involving both the Ga<sup>3+</sup> ions (disrupting the vital Fe<sup>3+</sup> metabolic pathway of bacteria) and Cu<sup>1+</sup> (*via* Fenton type reactions that produce ROS). The dual mechanism of attack also makes it unlikely that bacterial resistance will arise, an important quality in recent times where the occurrence of multidrug resistant bacterial is major concern. Furthermore, the synthesis of the highly transparent films carried out using the facile AACVD route allows the composite films to be easily applied to large surfaces at limited cost and difficulty.

## Acknowledgements

The EPSRC are thanked for studentship funding (IAH) through the Molecular Modelling and Materials Science Doctoral Training Centre (grant EP/G036675).

## References

- 1 V. Musat, B. Teixeira, E. Fortunato, R. C. C. Monteiro and P. Vilarinho, *Surf. Coat. Technol.*, 2004, **180**, 659–662.
- 2 M. W. Climo, D. S. Yokoe, D. K. Warren, T. M. Perl, M. Bolon, L. A. Herwaldt, R. A. Weinstein, K. A. Sepkowitz, J. A. Jernigan and K. Sanogo, *N. Engl. J. Med.*, 2013, **368**, 533–542.
- 3 K. Page, R. G. Palgrave, I. P. Parkin, M. Wilson, S. L. P. Savin and A. V. Chadwick, *J. Mater. Chem.*, 2007, **17**, 95–104.
- 4 S. Noimark, J. Weiner, N. Noor, E. Allan, C. K. Williams, M. S. P. Shaffer and I. P. Parkin, *Adv. Funct. Mater.*, 2015, **25**, 1367–1373.
- 5 I. A. Hassan, I. P. Parkin, S. P. Nair and C. J. Carmalt, *J. Mater. Chem. B*, 2014, **2**, 2855–2860.
- 6 A. M. Alotaibi, S. Sathasivam, S. P. Nair and I. P. Parkin, *J. Mater. Chem. B*, 2016, **4**, 666–671.
- 7 J. P. Ruparelia, A. K. Chatterjee, S. P. Duttagupta and S. Mukherji, *Acta Biomater.*, 2008, **4**, 707–716.
- 8 C. E. Santo, P. V. Morais and G. Grass, *Appl. Environ. Microbiol.*, 2010, **76**, 1341–1348.
- 9 C. E. Arnold, A. Bordin, S. D. Lawhon, M. C. Libal, L. R. Bernstein and N. D. Cohen, *Vet. Microbiol.*, 2012, **155**, 389–394.
- 10 M. Coleman, K. Kuskie, M. Liu, K. Chaffin, M. Libal, S. Giguère, L. Bernstein and N. Cohen, *Vet. Microbiol.*, 2010, **146**, 175–178.
- 11 C. R. Chitambar, *Future Med. Chem.*, 2012, **4**, 1257–1272.
- 12 C. R. Chitambar, D. P. Purpi, J. Woodliff, M. Yang and J. P. Wereley, *J. Pharmacol. Exp. Ther.*, 2007, **322**, 1228–1236.
- 13 M. Frezza, C. N. Verani, D. Chen and Q. P. Dou, *Letts. Drug Des. Discovery*, 2007, **4**, 311–317.
- 14 S. P. Valappil, D. Ready, E. A. A. Neel, D. M. Pickup, L. A. O'Dell, W. Chrzanowski, J. Pratten, R. J. Newport, M. E. Smith and M. Wilson, *Acta Biomater.*, 2009, **5**, 1198–1210.
- 15 N. Chadwick, S. Sathasivam, A. Kafizas, S. M. Bawaked, A. Y. Obaid, S. Al-Thabaiti, S. N. Basahel, I. P. Parkin and C. J. Carmalt, *J. Mater. Chem. A*, 2014, **2**, 5108–5116.
- 16 S. Ponja, S. Sathasivam, N. Chadwick, A. Kafizas, S. M. Bawaked, A. Y. Obaid, S. Al-Thabaiti, S. N. Basahel, I. P. Parkin and C. J. Carmalt, *J. Mater. Chem. A*, 2013, **1**, 6271–6278.
- 17 S. D. Ponja, S. Sathasivam, I. P. Parkin and C. J. Carmalt, *RSC Adv.*, 2014, **4**, 49723–49728.
- 18 S. Sathasivam, R. R. Arnepalli, K. K. Singh, R. J. Visser, C. S. Blackman and C. J. Carmalt, *RSC Adv.*, 2015, **5**, 11812–11817.
- 19 S. Sathasivam, R. R. Arnepalli, D. S. Bhachu, Y. Lu, J. Buckeridge, D. O. Scanlon, B. Kumar, K. K. Singh, R. J. Visser and C. S. Blackman, *J. Phys. Chem. C*, 2016, **120**, 7013–7019.
- 20 D. S. Bhachu, S. J. A. Moniz, S. Sathasivam, D. O. Scanlon, A. Walsh, S. M. Bawaked, M. Mokhtar, A. Y. Obaid, I. P. Parkin and J. Tang, *Chem. Sci.*, 2016, **7**, 4832–4841.
- 21 C. E. Knapp, I. D. Prassides, S. Sathasivam, I. P. Parkin and C. J. Carmalt, *ChemPlusChem*, 2014, **79**, 122–127.



- 22 B. Cheng and E. T. Samulski, *J. Mater. Chem.*, 2001, **11**, 2901–2902.
- 23 S. Sathasivam, R. R. Arnepalli, B. Kumar, K. K. Singh, R. J. Visser, C. S. Blackman and C. J. Carmalt, *Chem. Mater.*, 2014, **26**, 4419–4424.
- 24 M. C. Biesinger, L. W. M. Lau, A. R. Gerson and R. S. C. Smart, *Appl. Surf. Sci.*, 2010, **257**, 887–898.
- 25 A. M. Alotaibi, S. Sathasivam, S. P. Nair and I. P. Parkin, *J. Mater. Chem. B*, 2016, **4**, 666–671.
- 26 H. He, M. A. Blanco and R. Pandeyb, *Appl. Phys. Lett.*, 2006, **88**, 261904.
- 27 E. A. Albanesi, S. J. Sferco, I. Lefebvre, G. Allan and G. Hollinger, *Phys. Rev. B: Condens. Matter Mater. Phys.*, 1992, **46**, 13260.
- 28 A. Gaur, B. D. Shrivastava and S. K. Joshi, *J. Phys.: Conf. Ser.*, 2009, **190**, 012084.
- 29 L. S. Kau, D. J. Spira-Solomon, J. E. Penner-Hahn, K. O. Hodgson and E. I. Solomon, *J. Am. Chem. Soc.*, 1987, **109**, 6433–6442.

